06

Highly transient stimulated Raman scattering on high- and low-frequency phonon resonances of a $Sr_{0.9}Ba_{0.1}MoO_4$ crystal

© Yu.A. Kochukov[1,2], K.A. Gubina[1,2], D.P. Tereshchenko[1], A.G. Papashvili[1], V.E. Shukshin[1], I.S. Voronina[1], L.I. Ivleva[1], A.A. Ushakov[1], V.V. Bulgakova[1], P.A. Chizhov[1], S.N. Smetanin[1,2]

[1] Prokhorov General Physics Institute, Russian Academy of Sciences, Moscow, Russia
[2] National University of Science and Technology MISiS, Moscow, Russia

e-mail: axiniy@list.ru

Received December 26, 2024
Revised January 21, 2025
Accepted February 28, 2025

An investigation of stimulated Raman scattering (SRS) in a crystal of a $Sr_{0.9}Ba_{0.1}MoO_4$ cationic solid solution under subpicosecond laser pumping with pulse energy of 20 μJ and duration 0.25–6 ps with a controllable chirp is presented. Highly transient SRS with combined (high- and low-frequency) shifts and a small wavelength spacing not only in Stokes, but also anti-Stokes spectral region is observed due to increasing the integral scattering cross section for the secondary low-frequency Raman mode than for the primary high-frequency Raman mode in comparison with an initial $SrMoO_4$ crystal. Under optimum conditions, the first-order Stokes output pulse energy has reached 2.1 and 2.2 μJ with a supercontinuum part of 9% and 30% for high- and low-frequency shifts respectively. Analysis of spectral and temporal structure of output SRS radiation showed stronger influence of competitive nonlinear phenomena of self- and cross-phase modulation on SRS with the low-frequency shift. With negative chirping of the pump pulse, a sharp compression of the pulse of the first-order Stokes component with a low-frequency shift (up to 2.77 times) occurred with an abnormal shift of its spectral line to the short-wave region in comparison with the first Stokes component with the high-frequency shift.

Keywords: stimulated Raman scattering, highly transient regime, solid solution, pulse duration, self-phase modulation, cross-phase modulation.

DOI: 10.61011/EOS.2025.03.61158.11-25

Introduction

At present, new methods of multicolor two- or three-photon laser excitation of fluorophores or photosensitizers introduced into living tissues are being actively developed to increase the localization and efficiency of laser application in various biomedical diagnostic and treatment tasks [1,2]. This creates the need to develop multiwavelength sources of ultrashort radiation pulses with wavelengths lying in the first (650–950 nm), second (1000–1350 nm) or third (1600–1870 nm) therapeutic window of transparency of biological tissues [3]. The use of ultrashort pulse simulated Raman scattering (SRS) lasers, in which SRS radiation with a wavelength of 1240 nm was generated in addition to pumping laser radiation with a wavelength of 1050 nm, has previously shown an increase in the depth and contrast of multiphoton microscopy of living tissues [4,5] due to the simultaneous excitation of several multicolored fluorophores. A significant increase of the number of spectral components of laser radiation in the second (1000–1350 nm) therapeutic window of transparency of biological tissues has been previously realized at SRS in scheelite-like crystals of $MeMoO_4$ and $MeWO_4$ (Me is a divalent metal) due to the presence of not only primary but also secondary phonon resonance, and the creation of anionic solid solutions $Me(MoO_4)_{1-x}(WO_4)_x$ (x is the adjustable relative content) on their basis made it possible to further enrich the spectrum of the generated SRS radiation due to the control of the characteristics of the combined phonon resonances [6–9].

This article is devoted to the study of the characteristics of SRS radiation generated in a new cationic solid solution crystal $Sr_{0.9}Ba_{0.1}MoO_4$, in which the integral scattering cross section for the secondary low-frequency vibrational mode is increased relative to that for the primary high-frequency vibrational mode in comparison with the original $SrMoO_4$ crystal. This provided multicomponent SRS generation with a small wavelength spacing at a combined (high-frequency and low-frequency) frequency shift not only in the Stokes but also in the anti-Stokes region of the spectrum in the highly transient SRS regime, in which the duration of the pump pulse is commensurate with or shorter than the phase relaxation time of phonon resonances, which is realized by pumping with a subpicosecond ytterbium laser (1030 nm) with adjustable chirping of radiation pulses.

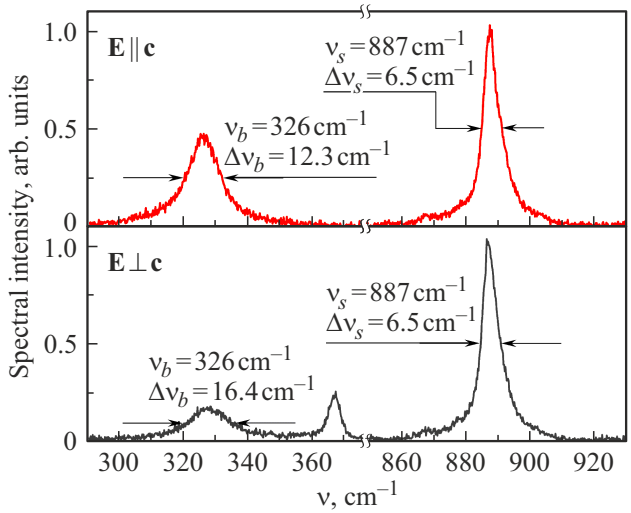

Figure 1. Polarized Raman spectra of a single crystal $Sr_{0.9}Ba_{0.1}MoO_4$ at **E** ∥ **c** (top) and **E** ⊥ **c** (bottom).

Description of material and experimental methodology

A crystal of strontium-barium molybdate in the proportion 9:1 of optical quality was grown at the Research Center for Laser Mate rials and Technology, Prokhorov General Physics Institute of the Russian Academy of Sciences by the Czochralski method from a platinum crucible in air in the direction [100]. Fig. 1 shows its polarized Raman spectra recorded during the propagation of excitation light polarized parallel (**E** ∥ **c**) and perpendicular (**E** ⊥ **c**) to the optical axis of the crystal. Both modes experienced noticeable broadening in comparison with the original $SrMoO_4$ crystal: $\Delta\nu_s$ from 2.6 cm^{-1} to 6.5 cm^{-1} (in both scattering geometries), and $\Delta\nu_b$ from 10.5 to 12.3 cm^{-1} at **E** ∥ **c** and to 16.4 cm^{-1} at **E** ⊥ **c**, which in principle should have a positive effect on the competitiveness of the secondary vibrational mode in the highly transient SRS regime. However, under the condition **E** ⊥ **c**, the relative intensity of ν_b-mode is much lower ($I_b/I_s = 0.17$) than that of **E** ∥ **c** ($I_b/I_s = 0.48$). Then assuming the steady-state Raman gain with pumping wavelength of $\lambda_p \approx 1\,\mu$m for the high-frequency mode g_s to be 2.24 cm/GW (in $\Delta\nu_b(Sr_{0.9}Ba_{0.1}MoO_4)/\Delta\nu_b(SrMoO_4)$ times smaller than for $SrMoO_4$ [9]), we obtain $g_b = g_s I_b/I_s = 1.9$ cm/GW at **E** ∥ **c** and only 0.37 cm/GW at **E** ⊥ **c**. Therefore, even with a larger increase of the width of the secondary vibrational mode, the value of $g_b\Delta\nu_b$, which is responsible for the SRS amplification in the highly transient regime, remains quite low (6.06 GW^{-1}) in the scattering geometry **E** ⊥ **c**. A noticeably better result is obtained under the condition **E** ∥ **c**. When reducing g_s to 2.24 cm/GW and keeping $g_s\Delta\nu_s$ at the same level (14.6 GW^{-1}) compared to the original strontium molybdate crystal, we obtain g_b and $g_b\Delta\nu_b$ higher (1.9 cm/GW and 23.4 GW^{-1}, respectively), which makes the low-frequency mode in the cationic solid solution under the condition **E** ∥ **c** more competitive and increases the chances of multiwavelength SRS generation.

The SRS experiment was carried out with pumping with ytterbium femtosecond fiber laser ANTAUS-10W-20u/1M (AVESTA Ltd, Russia) with a wavelength of 1030 nm, the radiation of which was focused into the center of a 6.5 cm long $Sr_{0.9}Ba_{0.1}MoO_4$ SRS-active element with antireflection coatings on the plane-parallel ends. When a focusing lens with $f = 8$ cm was used, the beam radius in the waist zone at the level of e^{-2} was 40 μm. The energy in the pumping pulses following with a frequency of 20 Hz was maintained at the level of 20 μJ, and their duration was varied from a minimum $\tau_0 = 0.25$ ps to a maximum $\tau_p = 6$ ps using the laser pulse chirping system integrated in the pumping laser. The polarization of the input radiation was controlled using a half-wave plate. The spectrum of the output SRS radiation was recorded with Ocean Optics USB4000 spectrometer operating in the range from 650 to 1150 nm and having a spectral resolution of 0.5 nm. The pulse energy values were recorded with an Ophir power and energy meter with a PE9-C pyroelectric sensor, and their duration was estimated using a scanning autocorrelator IRA-VISIR (AVESTA Ltd., Russia). The recorded autocorrelation curves were approximated by a Gaussian curve with a width at half maximum of the peak τ_{AC} corresponding to the true pulse duration $\tau_{pulse} = 0.707\tau_{AC}$. To study the characteristics of an individual component, the SRS radiation was first spatially separated using a reflective diffraction grating with a period of 600 mm^{-1} and reflectance of 67% in the first diffraction order.

Experimental results and discussion

Fig. 2 shows the spectra of anti-Stokes and Stokes components of the SRS radiation for the studied cationic solid solution of $Sr_{0.9}Ba_{0.1}MoO_4$ with pumping laser pulse durations of $\tau_p = 0.25$, 1, 3 and 6 ps obtained with negative and positive chirping. It can be seen from Fig. 2 that on the supercontinuum pedestal, which is higher at shortening of τ_p, multiwavelength SRS generation occurs in both the Stokes (1066, 1104, and 1134 nm) and anti Stokes (871, 889, 916, 944, 965, and 997 nm) regions of the spectrum. The identification of the frequency shifts for each component of the SRS radiation is also shown in Fig. 2. It should be noted that, compared to the original $SrMoO_4$ crystal [8], the new $Sr_{0.9}Ba_{0.1}MoO_4$ crystal exhibits the generation of an additional band around the wavelength of 1100 nm, which evolves into a SRS component at $\lambda_{bb} = [\lambda_p^{-1} - (\nu_b + \nu_b)]^{-1} = 1104$ nm with $\tau_p = 3$ ps excitation. This can be explained by the increase of the value of $g_b\Delta\nu_b$ and the decrease of the threshold intensity of nonlinear phase capture for the parametric

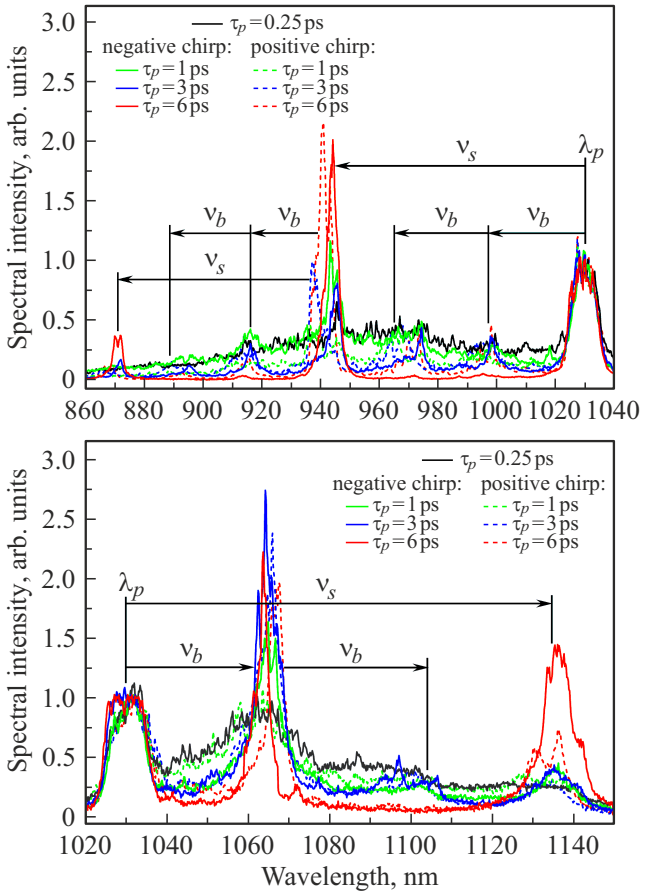

Figure 2. SRS radiation spectra of the anti-Stokes (top) and Stokes (bottom) regions for the single crystal $Sr_{0.9}Ba_{0.1}MoO_4$ with pump pulse durations of 0.25, 1, 3, and 6 ps obtained by negative (solid lines) and positive (dashed lines) chirping.

Raman interaction on the low-frequency vibrational mode due to the increase of g_b [10].

It is also possible to note in Fig. 2 (bottom) that the $\lambda_s = (\lambda_p^{-1} - \nu_s)^{-1} = 1134$ nm component shifts to the short-wave (long-wave) region of the spectrum at positive (negative) chirping of the pump pulse, which is explained by the origin of SRS „in the tail" of the pump pulse in the transient regime [11]. However, for the $\lambda_b = [\lambda_p^{-1} - \nu_b]^{-1} = 1066$ nm component, this trend is violated, indicating a stronger influence of competing nonlinear effects associated with the nonlinear refractive index on the low-frequency-shifted SRS process. The obtained measurements of time characteristics (Fig. 3) for the considered components confirm this assumption. When the pump pulse is negatively chirped, the SRS pulses are more strongly compressed at low-frequency shift than at high-frequency shift. Thus, while at the wavelength of $\lambda_s = 1134$ nm the durations of SRS pulses have a weak dependence on the chirp sign for any pump pulse duration, at $\lambda_b = 1066$ nm this dependence becomes significant. For instance, with $\tau_p = 4$ ps, positive and negative chirping yielded SRS pulse durations of 3.01 ps and 1.39 ps respectively — a 2.16-fold difference. Similarly, for $\tau_p = 6$ ps, the durations were 5.65 ps and 2.04 ps — a 2.77-fold difference. This clearly indicates a better compensation of the positive chirp caused by the nonlinear phenomena of self-phase modulation of pump radiation and cross-phase modulation of SRS radiation by the negative chirp of pump pulses in the case of SRS with low-frequency shift in comparison with high-frequency shift. It should be noted that the compression of SRS pulses observed at relatively long pump pulses of $\tau_p \geq 4$ ps, cannot be caused by group velocity mismatch of the pump and SRS pulses, since temporal walk-off length $L_{\text{GVM}} = \tau_p/\text{GVM}$ (GVM — group velocity mismatch) significantly exceeds the length of the SRS crystal. For example, based on the data on the refractive index dispersion of the related crystal $SrMoO_4$ [12] we have $\text{GVM}(\lambda_p, \lambda_b) = 9$ fs/mm and $\text{GVM}(\lambda_p, \lambda_s) = 24$ fs/mm, then we obtain $L_{\text{GVM}} \geq 444$ and 167 mm, respectively, at $\tau_p \geq 4$ ps. It also cannot be caused by the group velocity dispersion having values of $\text{GVD}(\lambda_b) = 147$ fs^2/mm and $\text{GVD}(\lambda_s) = 135$ fs^2/mm (again for $SrMoO_4$), giving very large temporal walk-off length $L_{\text{GVD}} = \tau_0^2/\text{GVD}$ of $L_{\text{GVD}} = 425$ and 464 mm, respectively ($\tau_0 = 0.25$ ps). Moreover, a fine structure of sub-pulses is observed for λ_b-component with pump pulse duration $\tau_p \geq 4$ ps, which indicates the splitting of the SRS pulse under the action of nonlinear phenomena related to the nonlinear refractive index. The reason for the smaller impact of these nonlinear phenomena on the formation of the high-frequency-shifted component of the SRS lies in the reduction of the phase mismatch of SRS interaction due to the mutual compensation of the self-phase modulation of the pump radiation and the cross-phase modulation of the SRS radiation [13]. It should also be noted that subpicosecond SRS radiation was obtained at $0.25\,\text{ps} \leq \tau_p \leq 1$ ps, but the pulse durations were close to 1 ps over this entire range of τ_p, and the height of the supercontinuum pedestal was commensurate with the intensity of the SRS peaks, which is attributable to the strong self-phase modulation of the pump radiation and the cross-phase modulation of the SRS radiation.

Fig. 4 shows the dependences of the energy in SRS pulses on the pump pulse duration for the same two SRS components, which are similar to those for the initial crystal of strontium molybdate [8]. Fig. 4 also shows the fraction of the supercontinuum pedestal in the measured energies, as estimated based on the results of spectral measurements. It can be seen that for both SRS components, with increasing pump pulse duration, the fraction of supercontinuum decreases and, consequently, the fraction of pure SRS increases, with the curve for a positively chirped pump pulse located 5–10% above the curve for a negatively chirped pump pulse, which is most pronounced for the component with a high-frequency shift. Fig. 4, *a* shows that when increasing the pump pulse duration to 6 ps (negative chirp), the λ_s component exhibits an increase in

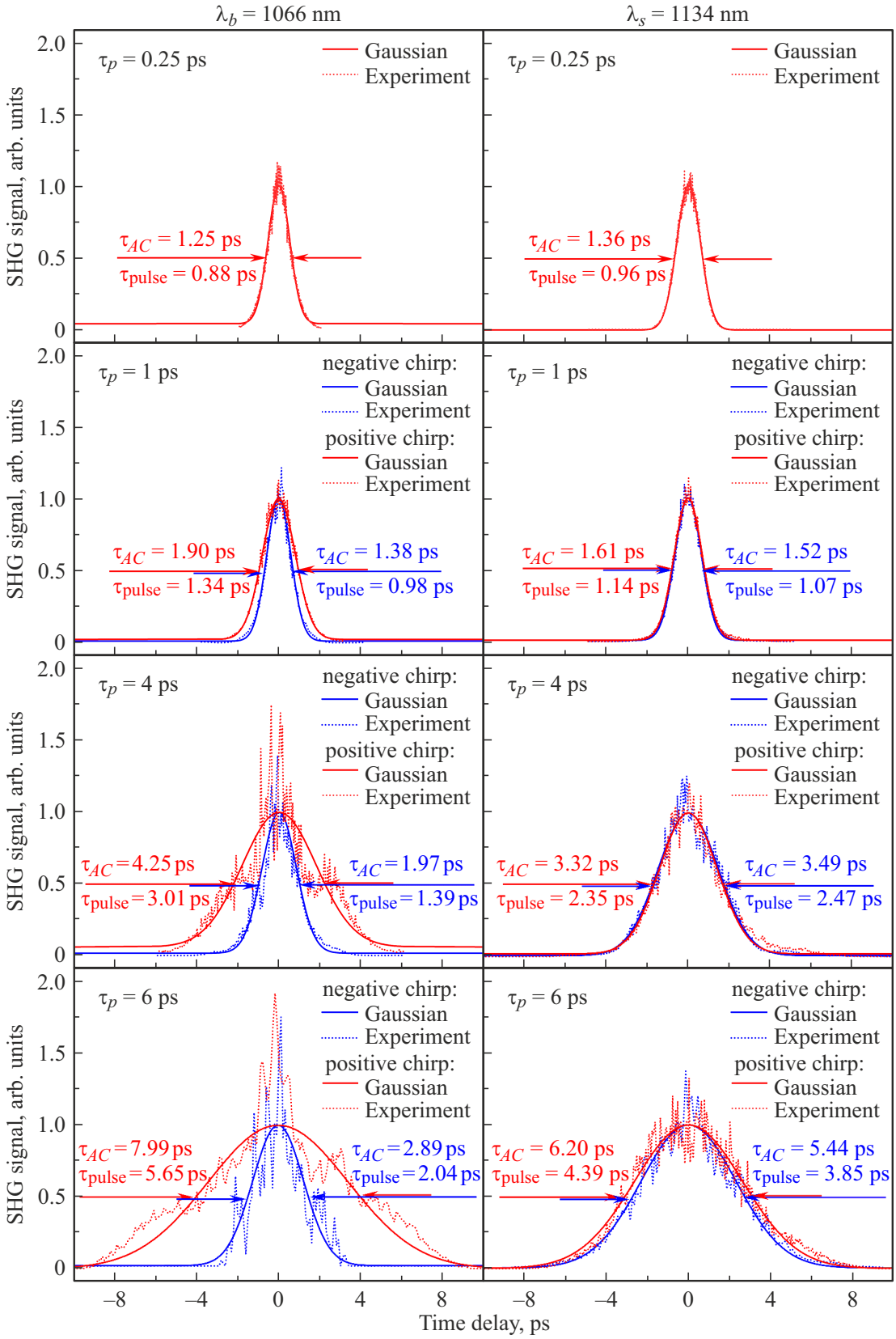

Figure 3. Autocorrelation curves for the SRS components of $\lambda_b = 1066$ nm and $\lambda_s = 1134$ nm with pump pulse durations of 0.25, 1, 4, and 6 ps obtained by negative (blue lines) and positive (red lines) chirping.

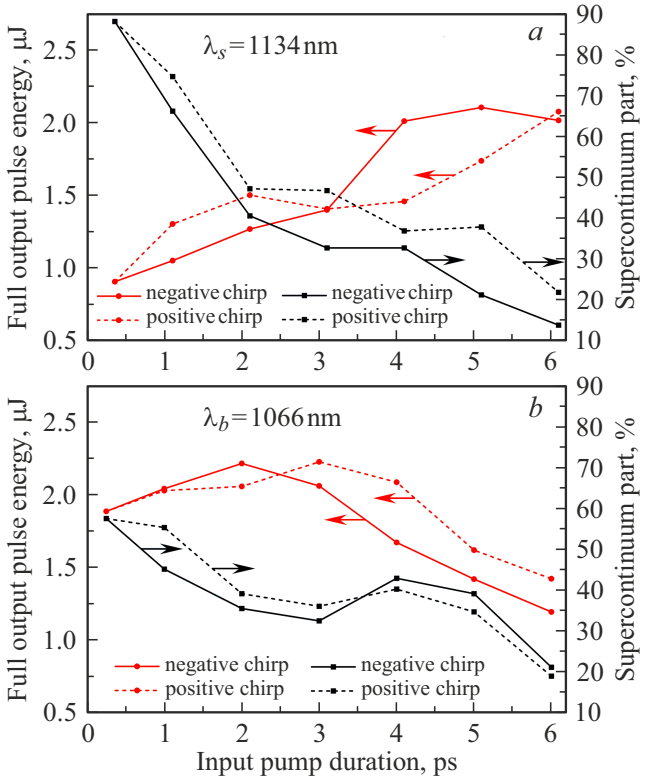

Figure 4. The total (SRS + supercontinuum) output energy in the pulse (red lines) and the fraction of supercontinuum in it (black lines) as a function of pump pulse duration for the SRS components: *a* — λ_s = 1134 nm, *b* — λ_b = 1066 nm. The energy measurement error did not exceed 10%.

pulse energy up to 2.1 μJ (SRS + supercontinuum part in the vicinity of λ_s) with a reduction of the supercontinuum fraction to 9%. This can be attributed to weakened effects of self- and cross-phase modulation [9,13]. In turn, Fig. 4, *b* shows that some optimal range from 1 to 4 ps is observed for the λ_b-component, which is attributable to the competition not only with self- and cross-phase modulation, but also with the SRS process on the high-frequency mode [9]. It should be noted that this optimal range exhibits not only the maximum of the pulse energy of the λ_b-component — 2.2 μJ (SRS + supercontinuum part in the vicinity of λ_b), but also the local minimum of the supercontinuum fraction of about 30%. Discussing the energy of the SRS radiation of the anti-Stokes region of the spectrum, it should be noted that the energy in the pulse for the 944, 965, and 997 nm components was of the order of 1 μJ, while it was an order of magnitude lower for the others.

Conclusion

This paper presents a study of the characteristics of the SRS radiation generated in the crystal of the cationic solid solution of $Sr_{0.9}Ba_{0.1}MoO_4$ when a highly transient SRS is realized. At **E** ∥ **c**, the increase of parameters g_b and $g_b\Delta\nu_b$ to 1.9 cm/GW and 23.4 GW^{-1}, respectively, compared to the original $SrMoO_4$ crystal, resulted in multiwavelength SRS generation with combined frequency shifts in both Stokes and anti-Stokes regions. Spectral and temporal measurements also demonstrated a stronger impact of the competing nonlinear phenomena related to the nonlinear refractive index on the low-frequency shift component of the SRS and the use of negative chirping of the pump pulse made it possible to compress its radiation pulse by a factor of more than 2 times compared to positive chirping owing to the compensation of the positive chirp attributable to self- and cross-phase modulation.

Funding

This study was financially supported by grant № 24-12-00448 from the Russian Science Foundation.

Conflict of interest

The authors declare that they have no conflict of interest.

References

[1] A.J. Bares, M.A. Mejooli, M.A. Pender, S.A. Leddon, S. Tilley, K. Lin, J. Dong, M. Kim, D.J. Fowell, N. Nishimura, C.B. Schaffer. Optica, **7** (11), 1587 (2020). DOI: 10.1364/optica.389982

[2] V. Juvekar, D.J. Lee, T.G. Park, R. Samanta, P. Kasar, C. Kim, F. Rotermund, H.M. Kim. Coord. Chem. Rev., **506**, 215711 (2024). DOI: 10.1016/j.ccr.2024.215711

[3] L.A. Sordillo, Y. Pu, S. Pratavieira, Y. Budansky, R.R. Alfano. J. Biomed Opt., **19** (5), 056004 (2014). DOI: 10.1117/1.jbo.19.5.056004

[4] Sh.A. Engelmann, A. Zhou, A.M. Hassan, M.R. Williamson, J.W. Jarrett, E.P. Perillo, A. Tomar, D.J. Spence, Th.A. Jones, A.K. Dunn. Biomed. Opt. Express, **13**, 1888 (2022). DOI: 10.1101/2021.10.20.464141

[5] E.P. Perillo, J.W. Jarrett, Y. Liu, A. Hassan, D.C. Fernée, J.R. Goldak, A. Bonteanu, D.J. Spence, H. Yeh, A.K. Dunn. Light Sci. Appl., **6** (11), e17095 (2017). DOI: 10.1038/lsa.2017.95

[6] M. Frank, S.N. Smetanin, M. Jelínek, D. Vyhlídal, V.E. Shukshin, L.I. Ivleva, E.E. Dunaeva, I.S. Voronina, P.G. Zverev, V. Kubeček. Crystals, **9** (3), 167 (2019). DOI: 10.3390/cryst9030167

[7] M. Frank, S.N. Smetanin, M. Jelínek, D. Vyhlídal, M.B. Kosmyna, A.N. Shekhovstov, K.A. Gubina, V.E. Shukshin, P.G. Zverev, V. Kubecek. Crystals, **12** (2), 148 (2022). DOI: 10.3390/cryst12020148

[8] A.G. Papashvili, Y.A. Kochukov, D.P. Tereshchenko, S.N. Smetanin, P.D. Kharitonova, V.E. Shukshin, E.E. Dunaeva, I.S. Voronina, L.I. Ivleva. Opt. Lett., **48** (17), 4528 (2023). DOI: 10.1364/ol.499428

[9] Y.A. Kochukov, K.A. Gubina, D.P. Tereshchenko, S.N. Smetanin, A.G. Papashvili, P.A. Chizhov, A.A. Ushakov, V.E. Shukshin, E.E. Dunaeva, I.S. Voronina, L.I. Ivleva. Opt. Lett., **49** (19), 5575 (2024). DOI: 10.1364/ol.538841

[10] D.P. Tereshchenko, S.N. Smetanin, A.G. Papashvili, K.A. Gubina, Yu.A. Kochukov, S.A. Solokhin, M.N. Ershkov, E.V. Shashkov, V.E. Shukshin, L.I. Ivleva, E.E. Dunaeva, I.S. Voronina. Tech. Phys., **68** (4), 455–461 (2023). DOI: 10.21883/TP.2023.04.55936.270-22
[11] R.L. Carman, F. Shimizu, C.S. Wang, N. Bloembergen. Phys. Rev. A, **2** (1), 60–72 (1970). DOI: 10.1103/PhysRevA.2.60
[12] *Handbook of Optics. Volume IV: Optical Properties of Materials, Nonlinear Optics, Quantum Optics*, 3rd ed. (The McGraw-Hill Companies, Inc., N.Y., 2010).
[13] A.V. Konyashchenko, P.V. Kostryukov, L.L. Losev, V.S. Pazyuk. Quant. Electron., **47** (7), 593–596 (2017). DOI: 10.1070/qel16404

Translated by A.Akhtyamov